Elasticity of Nanoparticles Influences Their Blood Circulation, Phagocytosis, Endocytosis, and Targeting

Aaron C. Anselmo, Mengwen Zhang, Sunny Kumar, Douglas R. Vogus, Stefano Menegatti, Matthew E. Helgeson,* and Samir Mitragotri*

Department of Chemical Engineering, Center for Bioengineering, University of California, Santa Barbara, California 93106, United States

ABSTRACT The impact of physical and chemical modifications of nanoparticles on their biological function has been systemically investigated and exploited to improve their circulation and targeting. However, the impact of nanoparticles' flexibility (*i.e.*, elastic modulus) on their function has been explored to a far lesser extent, and the potential benefits of tuning nanoparticle elasticity are not clear. Here, we describe a method to synthesize polyethylene glycol (PEG)-based hydrogel nanoparticles of uniform size (200 nm) with elastic moduli ranging from 0.255 to 3000 kPa. These particles are used to investigate the role of particle elasticity on key functions including blood circulation time, biodistribution, antibody-mediated targeting, endocytosis, and phagocytosis. Our results demonstrate that softer nanoparticles (10 kPa) offer enhanced circulation and subsequently enhanced targeting compared to harder nanoparticles (3000 kPa) *in vivo*. Furthermore, *in vitro* experiments show that softer nanoparticles exhibit significantly reduced cellular uptake in immune cells (J774 macrophages), endothelial cells (bEnd.3), and cancer cells (4T1). Tuning nanoparticle elasticity potentially offers a method to improve the biological fate of nanoparticles by offering enhanced circulation, reduced immune system uptake, and improved targeting.

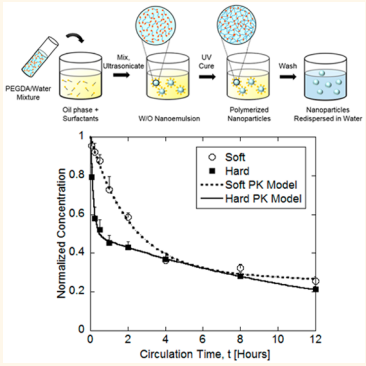

KEYWORDS: elasticity · nanogel · nanoemulsion · biodistribution · circulation · targeting · nanomedicine · nanoparticles

Physical attributes of nanoparticles such as morphology and elasticity have recently emerged as important parameters for the design of drug carriers. To improve upon key steps in the drug delivery process, such as circulation time, tissue targeting, barrier penetration, cellular uptake, and drug release, the physical properties of nanoparticles have been systematically investigated, and properties such as size, shape, material composition, and compartmentalization have all been shown to impact some of these key steps in the drug delivery process.[1,2] As such, recent research efforts have focused on leveraging these physical modifications to design nanoparticles capable of enhanced drug delivery. It is widely accepted that particle size is one of the most important physical parameters that can be tuned to dramatically alter the biological function of intravenously injected particles.[3−7] Indeed, nanoparticles (<500 nm) are more favored for intravenous drug delivery as they exhibit enhanced abilities to circulate, persist in blood, and target pathological tissues (*e.g.*, tumors), as compared to microparticles (>500 nm).[8] Following size, the shape of nanoparticles is the next most investigated physical parameter that can be tuned to improve a nanoparticle's biological functions.[9,10] It has been shown that shape can have dramatic effects on targeting, circulation, internalization, immune cell association, and adhesion.[11−19]

While systematic investigations have shed light on the role of size and shape on nanoparticle delivery abilities, relatively little is known about the role of carrier elasticity on drug delivery. The motivation for investigating elasticity of nanocarriers stems from a wide body of literature detailing the effects that material elasticity can have on biological systems.[20−22] For example, cell culture substrates of varying elasticity have been shown to direct and control cell fates, optimize cell growth, and even improve delivery of therapeutics.[23−26] While the benefits of tuning elasticity are widely investigated for cell culture substrates and scaffolds, similar studies are severely lacking for particle delivery systems

* Address correspondence to samir@engineering.ucsb.edu, helgeson@engineering.ucsb.edu.

Received for review January 9, 2015 and accepted February 25, 2015.

Published online February 25, 2015
10.1021/acsnano.5b00147

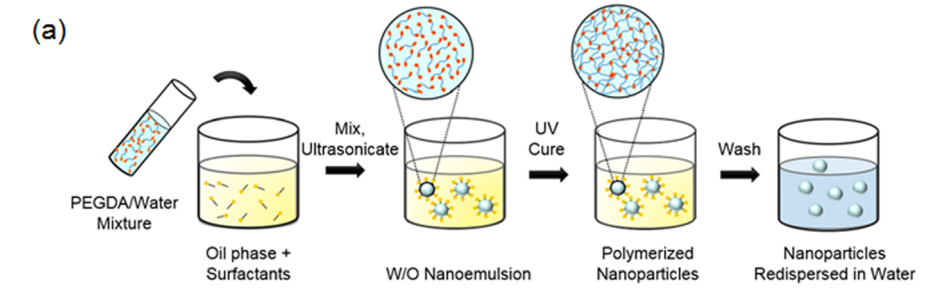

(b)

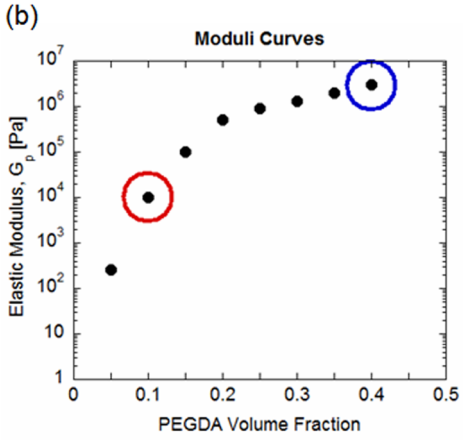

(c)

Parameter	Soft Particles	Hard Particles
Bulk Modulus [kPa]	10	3000
Diameter in Z-average [nm]	209	217
PDI	0.23	0.27
ζ-potential [mV]	-36.8 ± 9.2	-35.3 ± 9.0
Anti-ICAM [μg protein per trillion particles]	3.8 ± 0.8	4.1 ± 0.6

Figure 1. Soft and hard hydrogel nanoparticles. (a) Schematic representation of hydrogel nanoparticle synthesis. (b) Hydrogel nanoparticle elasticity can be tuned by varying PEGDA volume fraction. (c) Hydrogel nanoparticle properties for soft and hard nanoparticles.

as only a few studies have alluded to the role of particle elasticity in drug delivery processes.[12,27−29] Recent work reported the effect of elasticity over a range of 10 to 63.8 kPa on circulation and biodistribution of microparticles that are shaped like red blood cells.[27] It was shown that an 8-fold decrease in particle modulus resulted in a greater than 30-fold increase in the elimination half-life for the softer microparticles. A subsequent study investigated similar red-blood-cell-shaped particles as small as 800 nm and showed that microparticles similarly sized to red blood cells exhibited the longest circulation times.[28]

Here, we expand on these seminal findings by decoupling the tandem effects of shape and elasticity and assessing the role of elasticity on circulation and targeting for small spherical nanoparticles (~200 nm). We have developed an approach to synthesize hydrogel nanoparticles over a wide range of elasticity (0.255 to 3000 kPa) *via* a nanoemulsion (miniemulsion) templating method[30,31] and utilized these nanoparticles to identify the fundamental role that nanoparticle elasticity plays in facilitating cellular uptake, circulation, biodistribution, and targeting to tissues. We show that by tuning the elasticity of hydrogel nanoparticles it is possible to design carriers capable of enhanced circulation and targeting *in vivo*.

RESULTS

Synthesis and Characterization of Hydrogel Nanoparticles. Hydrogel nanoparticles composed of poly(ethylene glycol) diacrylate (PEGDA) with tunable elastic modulus were synthesized *via* a water/PEGDA-in-oil nanoemulsion (miniemulsion) templating method (Figure 1a). Given the benefits in particle stability and ease for scale up, nanoemulsion methods have been widely used as a templating method for synthesizing hydrogel nanoparticles[30,32,33] and provide a facile route for controlling particle elasticity independent of other particle properties (primarily size). Elastic moduli could be tuned over a range of 0.255 kPa to 3 MPa (Figure 1b) by changing the volume fraction of PEGDA in the nanoemulsion. Nanoparticles were also surface-functionalized with 2-carboxyethyl acrylate to facilitate conjugation with antibodies. Nanoparticles with two distinct moduli, soft (Figure 1b, circled in red) and hard (Figure 1b, circled in blue), were used for further studies. The extremely soft nanoparticles (modulus ~0.255 kPa) were not used due to their proximity to the minimum percolation threshold for gelation. "Soft" particles used in the study had an elastic modulus of 10 kPa (Figure 1c), and "hard" particles had an elastic modulus of 3 MPa (Figure 1c). Other properties of particles including size (~200 nm) and surface charge (~−35 mV) were kept constant (Figure 1c). Nanoparticles with these size and charge characteristics are widely used in preclinical settings, and thus their biological performance in terms of circulation, biodistribution, and targeting is well-known.[14,34] Additionally, fixing these other physical and chemical

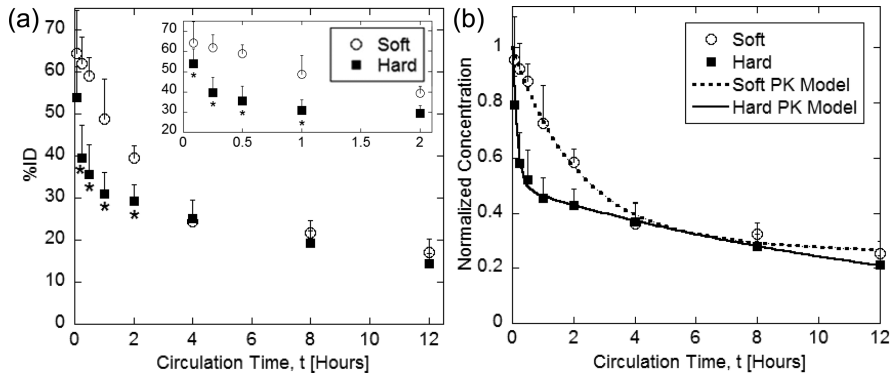

Figure 2. Blood circulation time course for soft and hard hydrogel nanoparticles. (a) Circulation data for both soft (open circles) and hard (black squares) hydrogel particles over a 12 h period. Inset highlights the same data at short times. (b) Two-compartment pharmacokinetic model for soft and hard hydrogel nanoparticles. Error bars represent SD (n = 4). *Denotes statistical difference (P < 0.05) using Student's t test between soft and hard hydrogel nanoparticle groups.

parameters between the soft and hard particles allows clearer investigation into the role of nanoparticle elasticity on *in vivo* drug delivery processes.

Circulation of Soft and Hard Hydrogel Nanoparticles. The role of nanoparticle elasticity on circulation time *in vivo* was investigated by intravenously injecting an identical number of radio-labeled soft and hard hydrogel nanoparticles into mice. Soft nanoparticles exhibited a significantly higher persistence in blood compared to hard nanoparticles at short times (Figure 2a and inset). However, this difference between the two particles is significantly reduced after 4 h. Both particle types showed a decay with two distinct time scales; therefore, pharmacokinetic parameters were determined using a standard two-compartment model (Figure 2b), $C = Ae^{\alpha t} + Be^{\beta t}$, as previously described,[27] and key circulation parameters were estimated (Supporting Information Figure S1). Specifically, the distribution half-life (α^{-1}), which describes nanoparticle distribution from plasma into tissues, and the elimination half-life (β^{-1}), which describes the kinetics of permanent nanoparticle clearance from plasma, were both found to be longer for soft nanoparticles compared to hard nanoparticles.

Biodistribution and Targeting of Soft and Hard Hydrogel Nanoparticles. The organ distributions of soft and hard hydrogel nanoparticles *in vivo* were investigated at representative short (30 min) and long (12 h) time points. At 30 min, significant differences in organ retention in the kidneys, heart, lungs, and brain were found when comparing soft and hard hydrogel nanoparticles (Figure 3a). At 12 h, these differences in organs nearly disappear, and soft nanoparticles and hard nanoparticles show statistically different organ distribution only in the lungs (Figure 3b). We attribute these time-dependent biodistribution differences to the different circulation times of the soft and hard nanoparticles. Specifically, the ability of softer nanoparticles to persist at higher concentrations for short time points (<2 h) likely results in greater retention of these particles in organs that receive higher blood output.

Soft and hard hydrogel nanoparticles were next conjugated with anti-ICAM antibody, a model antibody that has been widely used to investigate targeting to the lungs.[35] As such, anti-ICAM antibody can be used to probe the differences of soft nanoparticles and hard nanoparticles in targeting specific tissues. After 30 min, significant differences in organ accumulation between anti-ICAM antibody-conjugated soft and hard hydrogel nanoparticles were seen in the liver, spleen, heart, brain, lungs, and blood (Figure 3c). ICAM is a protein expressed basally on all endothelial cells, with the lungs and spleen expressing significantly more than other tissues.[36] Indeed, soft nanoparticles show significant increases in targeting to spleen and lungs over their harder counterparts. Similar enhancements were also seen in the heart and brain, as well. Relative accumulation of nanoparticles compared to blood concentration was determined by calculating lung-to-blood localization ratios. No significant differences between lung-to-blood localization ratios were seen between soft and hard nanoparticles with or without anti-ICAM targeting (Figure 3d). This comparison corroborates that enhanced lung targeting of soft nanoparticles is likely attributed to increased persistence in blood.

Cellular Uptake of Soft and Hard Nanoparticles. The impact of nanoparticle elasticity on cellular uptake *in vitro* was investigated in three different murine cell lines: (i) 4T1 epithelial tumor cells, (ii) bEnd.3 brain endothelial cells, and (iii) J774 macrophages. First, unmodified soft and hard nanoparticles were incubated with 4T1 epithelial tumor cells at time points matching the *in vivo* blood circulation studies. At short time points (5 min to 4 hr), no statistical differences in cellular uptake were observed; however, at 8 and 12 h, hard nanoparticles were bound/internalized to a greater extent than their soft counterparts, although the difference was relatively modest (Figure 4a). The effect of anti-ICAM antibody on uptake by 4T1 cells was also assessed. 4T1 cells are known to express ICAM receptors on their surface.[37] Anti-ICAM antibody increased

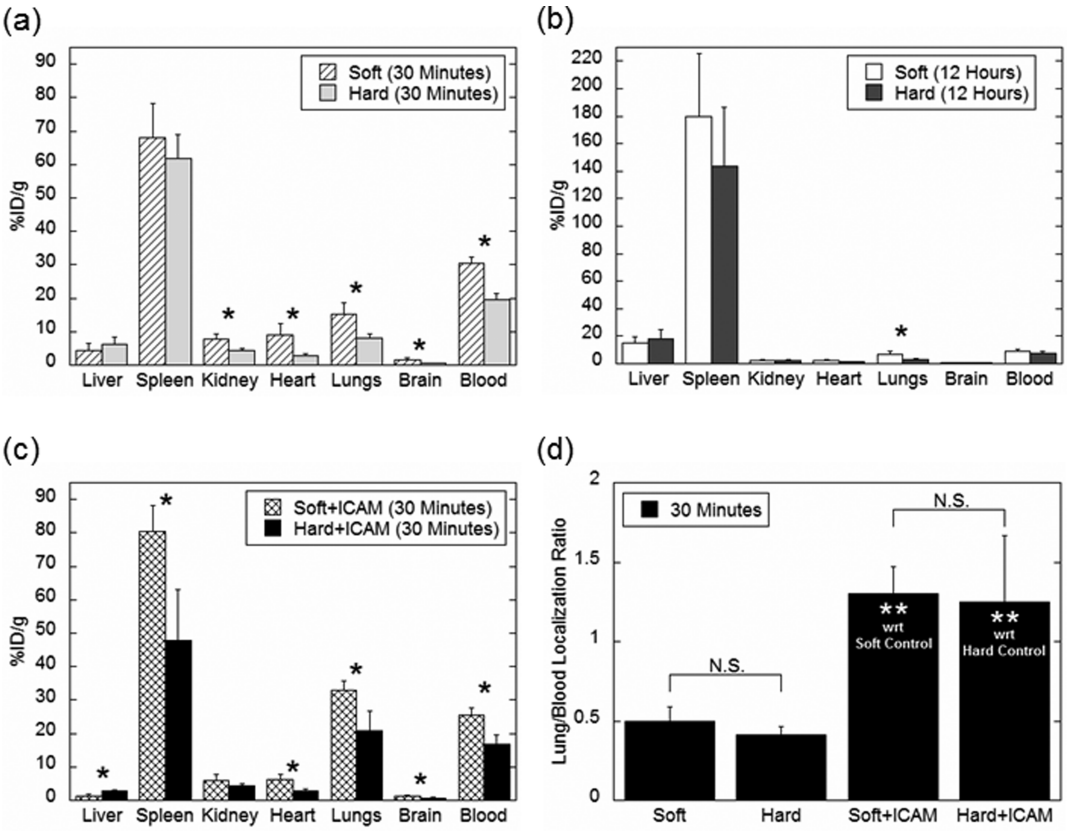

Figure 3. Biodistribution of soft and hard hydrogel nanoparticles. (a) Biodistribution in various organs of soft (hatched bars) and hard (light gray bars) hydrogel nanoparticles at 30 min. (b) Biodistribution in various organs of soft (white bars) and hard (dark gray bars) hydrogel nanoparticles at 12 h. (c) Biodistribution in various organs of soft + ICAM (cross hatched bars) and hard + ICAM (black bars) hydrogel nanoparticles at 30 min. (d) Lung-to-blood localization ratio for soft, hard, soft + ICAM, and hard + ICAM nanoparticles at 30 min. Error bars represent SD (n = 3 for 30 min time points and n = 4 for 12 h time point). *Denotes statistical difference (P < 0.05) using Student's t test between soft and hard hydrogel nanoparticle groups. **Denotes statistical difference (P < 0.05) using Student's t test between soft + ICAM or hard + ICAM groups and their respective bare soft and hard controls.

uptake of both soft and hard particles at all time points in 4T1 cells compared to unmodified nanoparticles (Figure 4b). Furthermore, statistical differences at additional time points (2, 4, 8, and 12 h) between 4T1 cellular uptake of anti-ICAM antibody-conjugated soft and hard nanoparticles was observed; specifically, hard nanoparticles were taken up to a much higher extent than their softer counterparts (Figure 4b), exacerbating the effects seen in the absence of the anti-ICAM antibody. It is possible that these differences in uptake between anti-ICAM antibody-conjugated particles and unmodified particles in 4T1 cells may also arise from changes in hydrophobicity or charge following antibody conjugation. Regardless, hard nanoparticles were still taken up to a much higher extent than their soft counterparts in both the targeted and nontargeted cases.

Uptake of anti-ICAM antibody-coated soft and hard nanoparticles in an endothelial cell line (bEnd.3) was also assessed. The bEnd.3 cells express high amounts of ICAM receptor[38] and were stimulated with lipopolysaccharide (LPS) to increase ICAM expression further (Supporting Information Figure S2)[39,40] to maximize the amount of ICAM receptor present on cell surfaces and subsequently to facilitate enhancement of receptor-mediated endocytosis compared to other internalization mechanisms. Similar to cellular uptake in 4T1 cells, hard nanoparticles exhibited increased uptake in LPS-stimulated bEnd.3 cells compared to soft nanoparticles (Figure 4c). Interestingly, significant increases in uptake for ICAM hard nanoparticles were seen at each time point, including 5 min (Figure 4c). It is likely that ICAM facilitates uptake *via* cell adhesion−molecule endocytosis in both 4T1 and bEnd.3 cells.[11]

Impact of elastic modulus on nanoparticle internalization by macrophages was also studied using the J774 macrophage cell line. To facilitate phagocytosis, mouse IgG antibody, which is known to interact with the Fc receptors on macrophage surfaces,[41] was conjugated to the surface of nanoparticles. Similar to the enhanced uptake/binding in both endothelial and epithelial cells, hard particles were phagocytosed at a significantly higher quantity than soft nanoparticles in J774 macrophages (Figure 4d). In some cases (12 h), the increase in the number of hard particles phagocytosed is greater than 3.5-fold. This internalization in macrophages was visually confirmed by labeling of nanoparticles (Supporting Information Figure S3). These *in vitro* studies indicate that hard nanoparticles are endocytosed

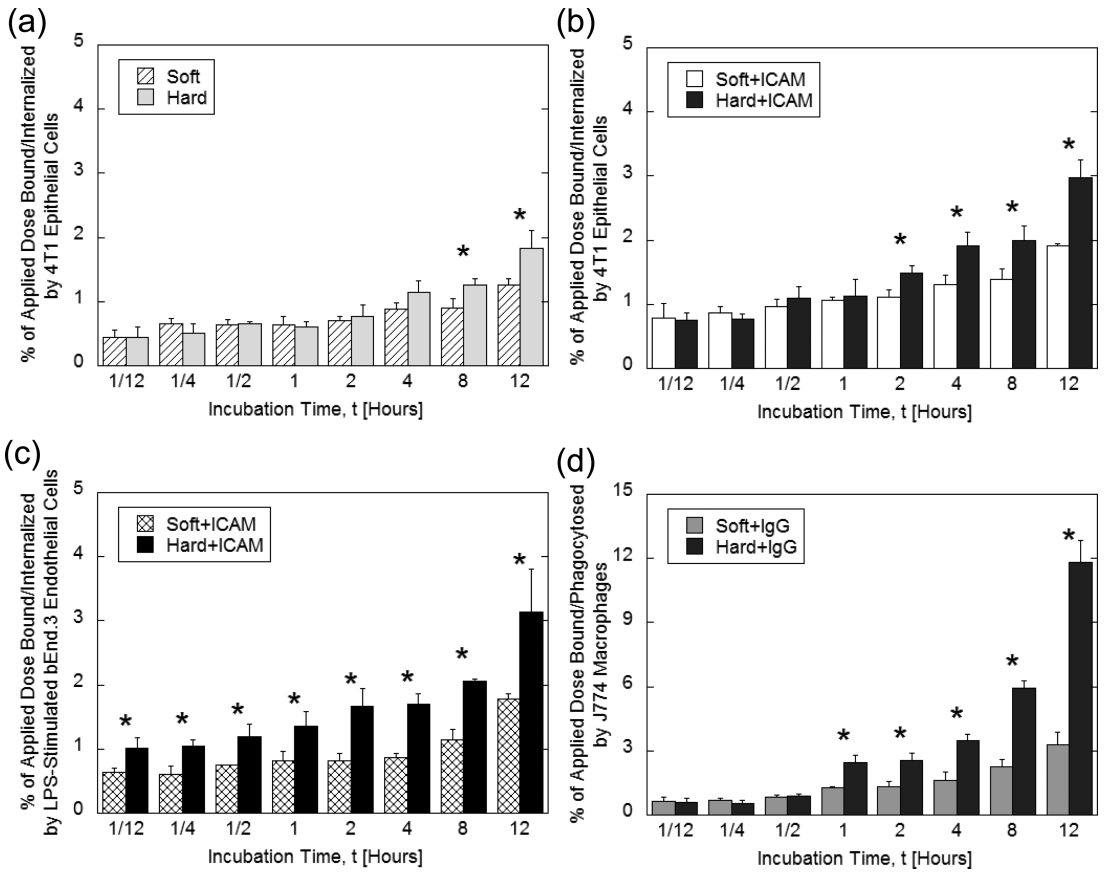

Figure 4. Cellular uptake of soft and hard hydrogel nanoparticles. (a) Cellular uptake of bare soft (hatched bars) and hard (light gray bars) hydrogel nanoparticles in 4T1 epithelial cells at various time points. (b) Cellular uptake of ICAM-conjugated soft (white bars) and hard (dark gray bars) hydrogel nanoparticles in 4T1 epithelial cells at various time points. (c) Cellular uptake of ICAM-conjugated soft (cross hatched bars) and hard (black bars) hydrogel nanoparticles in LPS-stimulated bEnd.3 endothelial cells at various time points. (d) Cellular uptake of mouse IgG-conjugated soft (light gray bars) and hard (dark gray bars) hydrogel nanoparticles in J774 macrophages at various time points. Error bars represent SD (n = 3). *Denotes statistical difference (P < 0.05) using Student's t test between soft and hard hydrogel nanoparticle groups.

(Figure 4a−c) to a higher extent and more rapidly than their softer counterparts. Furthermore, hard particles are phagocytosed (Figure 4d and Figure S3) to an even higher rate and in higher amounts than their softer counterparts, with the largest differences observed in macrophages.

DISCUSSION

This work demonstrates that modulation of nanoparticle elasticity offers a promising strategy to alter the circulation time, biodistribution, and cellular internalization of nanoparticles. The nanoemulsion technique employed here allowed for synthesis of PEG-based hydrogel nanoparticles with tunable elasticity, while keeping all other parameters (size, shape, charge) constant. By varying the PEGDA volume fraction, the stiffness of nanoparticles could be controlled. In this particular study, the volume fraction of PEGDA (M_n = 700 g/mol) was adjusted to control the elasticity of the nanoparticles over a wider range (0.255 kPa to 3 MPa) than was reported in previous studies.

Both soft (10 kPa) and hard (3 MPa) PEGDA hydrogel nanoparticles exhibited long circulation, likely due to the presence of PEG, which grants resistance to both opsonization and reticuloendothelial system clearance.[42,43] The soft nanoparticles persisted in the blood at a much higher concentration than the hard nanoparticles at short time points (<2 h), demonstrating the importance of elasticity in nanoparticle design (Figure 2a). A two-compartment pharmacokinetic model was fit to circulation data because both particle types showed decay with two distinct time scales, and the model showed strong agreement with the data (Figure 2b). The primary assumption of a two-compartment model is that the organism is simplified into a central compartment comprising organs with higher blood permeation (*e.g.*, heart) and a peripheral compartment comprising organs with lower blood permeation (*e.g.*, adipose tissue).[44] The model shows that estimated values for both distribution and elimination half-lives are higher for the softer nanoparticles than for the harder nanoparticles (Supporting Information Figure S1).

In order to investigate mechanisms as to why softer particles circulate longer than harder nanoparticles, *in vitro* macrophage phagocytosis experiments were used to determine the role nanoparticle elasticity

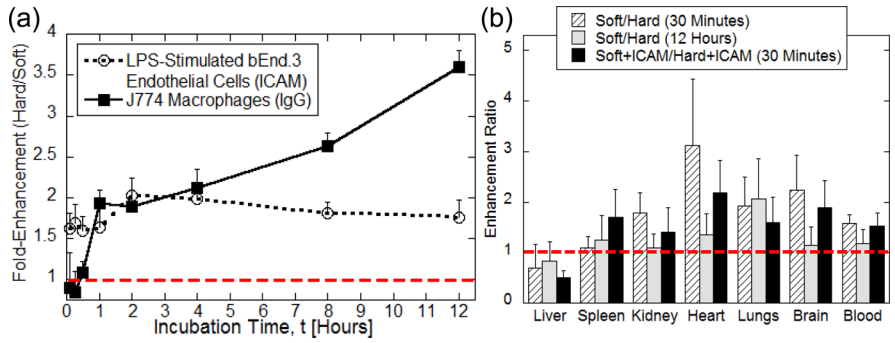

Figure 5. (a) Enhancement ratios (hard/soft) for *in vitro* cell uptake studies of ICAM-conjugated nanoparticles in LPS-stimulated bEnd.3 cells (open circles) and IgG-conjugated nanoparticles in J774 macrophages (closed squares). Error bars represent SD ($n = 3$). (b) Fold enhancement (soft/hard) in various organs at 30 min (hatched bars), 12 h (light gray bars), and at 30 min with ICAM conjugation to particles (black bars). Error bars represent SD ($n = 3$ for 30 min time point and $n = 4$ for 12 h time point).

played in avoiding phagocytosis. At 12 h, hard particles are phagocytosed over 3.5-fold more than their soft counterparts in J774 macrophages (Figure 4d and Figure S3). Interestingly, all *in vitro* cellular uptake experiments showed increased uptake of harder nanoparticles (Figure 5a and Figure S4). This enhanced uptake of stiffer particles is true for all cell lines studied here: (i) 4T1 epithelial cells (Figure 4a,b), (ii) LPS-stimulated bEnd.3 endothelial cells (Figure 4c), and (iii) J774 macrophages (Figure 4d). However, since this enhancement was most dramatic in phagocytotic macrophages (Figure 4d), where the enhancement ratio reached as high as 3.5 (Figure 5a), this may suggest that hard particles circulate for less time due to more rapid clearance by phagocytotic immune cells. Differences between short-term (~2 h) clearance of particles *in vivo* and peak phagocytosis of particles by macrophages at longer time points (~8 h) *in vitro* are attributed to a lack of physiological conditions *in vitro* such as flow, filtration systems (*e.g.*, spleen), and other phagocytotic immune cells (*e.g.*, monocytes) that facilitate clearance of particles. Differences in the kinetics of particle uptake *in vitro* and organ retention *in vivo*, especially at shorter times, likely stem from effects not considered in our *in vitro* system, such as effects related to flow, effects related to opsonization, and the extent of contact time between a given cell and a given particle.

Softer nanoparticles circulate longer than hard nanoparticles at short time points likely due to softer particles avoiding permanent clearance by macrophage-hosting reticuloendothelial organs. One possible reason for this enhanced binding and uptake of harder particles and longer circulation of softer particles is that the forces that phagocytotic cells, such as macrophages, exert on particles during phagocytosis may be sufficiently strong to deform the particles. Depending on how the particle deforms, the particle may deform in such a way that the particle's radius of curvature changes in the direction normal to the cell membrane. In this case, one possibility is that the extent of phagocytosis can potentially be decreased if the particle's shape becomes elongated or stretched.[18] Another possibility is that the extent of phagocytosis can potentially decrease due to an increase in the cell membrane tension that must be sustained in order to complete phagocytosis because it has been shown in some cases that phagocytosis is significantly reduced as the radius of curvature of spherical particles decreases.[45]

Biodistribution studies showed increased accumulation in certain organs at 30 min for soft nanoparticles compared to hard nanoparticles. This is best visualized by determining nanoparticle accumulation ratios (soft/hard) in each organ at each time point for each condition (Figure 5b). These increases of soft nanoparticles in organs at short time points are likely due to the increased blood persistence of soft nanoparticles, which results in increased retention of soft nanoparticles in organs that receive higher blood output (Figure 5b, hatched). The highest concentration of both soft and hard nanoparticles is seen in the spleen at 30 min (Figure 3a). While the concentration of both soft and hard nanoparticles is high in the spleen, the total percentage of the injected dose in the spleen is much lower (5.3 ± 0.4%ID for soft particles and 5.0 ± 0.1%ID for hard particles). Interestingly, the spleen shows high concentration of both soft and hard nanoparticles at a longer time point (Figure 3b), which suggests that the spleen is likely responsible for permanent clearance of both soft and hard nanoparticles. This hypothesis is further supported by the fact that the spleen does not receive high cardiac output/blood flow as compared to other organs. Furthermore, many other studies that have utilized similar modulus PEGDA hydrogel particles have seen preferential uptake in the spleen as compared to all other organs.[27,28]

CONCLUSION

In conclusion, this study demonstrates synthesis of two physically distinct nanoparticles that differ in elastic moduli (10 kPa *vs* 3 MPa) but are otherwise identical. These nanoparticles were used to explore the

impact of elasticity on drug delivery processes, notably blood circulation, biodistribution, tissue targeting, and cellular uptake in terms of both endocytosis and phagocytosis. Based on the studies reported here, several conclusions can be drawn: (i) soft nanoparticles are able to persist in circulation in higher amounts at short times compared to hard nanoparticles, and this can be used to increase targeting to certain tissues; (ii) at longer times, circulation differences between soft nanoparticles and hard nanoparticles are reduced; (iii) this increased blood persistence can be attributed to the ability of softer particles to resist phagocytosis for longer times than their harder counterparts; (iv) both soft and hard PEGDA hydrogel nanoparticles are eventually cleared by the spleen; and (v) harder particles are endocytosed much more rapidly and in higher amounts than softer nanoparticles, and this internalization trend is even more pronounced for immune cell phagocytosis. By tuning elasticity, softer particles could be potentially utilized to avoid endocytosis and phagocytosis and effectively provide benefits in circulation and targeting by increasing opportunities to bind to target sites due to increased blood persistence. However, if intracellular drug delivery or rapid cell internalization is desired, harder particles could be utilized to increase association with cells and increase particle uptake. These results suggest that elasticity of nanoparticles can be leveraged to improve key drug delivery abilities of nanoparticles, and perhaps, elasticity can be best utilized in tandem with modifications of other physical (*e.g.*, shape) and chemical (*e.g.*, targeting ligands) parameters to create more advanced nanoparticle delivery systems. Future studies will investigate the role that elasticity plays in both extravasation of nanoparticles through defects in endothelium and transcytosis through biological barriers.

METHODS

Particle Preparation. Poly(ethylene glycol) diacrylate (M_n = 700 g/mol), Span 80, Tween 80, 2-carboxyethyl acrylate, and 2-hydroxy-2-methylpropiophenone were acquired from Sigma-Aldrich. Methacryloxyethyl thiocarbamoyl rhodamine B (rhodamine methacrylate) was purchased from Polysciences. All materials were used as supplied. Hydrogel nanoparticles of various stiffness were synthesized following a nanoemulsion templating method (Figure 1a) as follows. The dispersed aqueous phase contains a mixture of PEGDA (10 vol % for the softest particles and 40 vol % for the stiffest particles), 2-carboxyethyl acrylate (1 vol %), and Millipore deionized (DI) water (89 vol % for the softest particles and 59 vol % for the stiffest particles). The fluorescent dye rhodamine methacrylate (0.1 wt %) was also incorporated into the mixture for all particle batches for ease of detection. The dispersed phase (1 mL) was emulsified into a continuous oil phase of cyclohexane (15 mL) containing the surfactants Span 80 (300 mg) and Tween 80 (100 mg) under strong stirring. The emulsion droplet size was then further homogenized using an ultrasonicator (Fisher Scientific model FB705) to produce nanodroplets. Photoinitiator 2-hydroxy-2-methylpropiophenone (80 μL) was then added to the nanoemulsion, and a 365 nm long-wave UV lamp was used to photocross-link PEGDA in the nanodroplets (15 min exposure) into hydrogel nanoparticles *via* free-radical polymerization. The nanoparticles were separated *via* centrifugation (18 000*g*) and washed into cyclohexane (three rounds) followed by Millipore DI water (five rounds). Finally, purified hydrogel nanoparticles were resuspended into DI water and stored at 6 °C for further use. Nanoparticle concentrations were determined by freeze-drying a known volume of sample and measuring its final freeze-dried mass.

Radio-labeling of nanoparticles was performed by activating 1.5×10^{13} particles in 10 mg/mL of 1-ethyl-3-(3-(dimethylamino)propyl)carbodiimide (EDC) in 2-(*N*-morpholino)-ethanesulfonic acid (MES) buffer for 15 min under constant rotation at room temperature (Supporting Information Figure S5). Particles were then washed *via* centrifugation at 15 000*g* and resuspended in MES buffer. 3H-Glycine was added in excess and allowed to react with particles for 8 h at room temperature. Following 3H-glycine conjugation, particles were washed a total of 10 times *via* centrifugation at 15 000*g* in saline to remove excess 3H-glycine.

Hydrogel Modulus. The elastic moduli of PEGDA hydrogels were measured using an AR-G2 rheometer (TA Instruments) at room temperature using an accessory for simultaneous UV exposure and rheological measurement within a 25 mm parallel plate geometry with a gap space of 800 μm. To investigate the effect of PEGDA volume fraction on gel elasticity, samples were prepared at various concentrations of PEGDA in water (5 to 40 vol %) with the addition of 1 vol % of photoinitiator. After the bulk gel was polymerized using the UV assembly (20 s UV exposure, 150 mV/cm^2 irradiation), frequency sweeps were performed (0.01 to 50 Hz) at a strain rate of 0.05% to quantify the gel's plateau modulus (G_p).

Particle Sizing and ζ-Potential Measurements. Size measurements were obtained by dynamic light scattering using a Malvern Zetasizer Nano ZS at room temperature. The light scattering was measured using noninvasive backscatter optics, and the resulting autocorrelation function was used to determine the *Z*-average diameter of particles. To ensure adequate particle sizing, each sample was diluted with filtered Millipore DI water to 10^{-2}% mass and measured three times. ζ-Potential measurements were performed for three runs per sample (12 measurements per run) in DI water using a Malvern Zetasizer at room temperature.

Antibody Conjugation. Following conjugation of glycine, glycine-modified nanoparticles were activated with EDC at a concentration of 0.1 mg/mL in MES for 15 min under constant rotation at room temperature (Supporting Information Figure S6). Particles were then washed *via* centrifugation at 15 000*g* and resuspended in phosphate-buffered saline (PBS). Anti-ICAM-1 or mouse IgG antibodies were added at a concentration of 400 μg/mL in PBS to an identical concentration of soft and hard nanoparticles and allowed to react with particles for 8 h at room temperature. Following antibody conjugation, particles were washed a total of 10 times *via* centrifugation at 15 000*g* in saline to remove excess antibody.

***In Vivo* Biodistribution and Circulation.** Particles (3×10^{12}) in 100 μL of saline were injected into the tail vein of healthy female BALB/c mice (18−20 g). At various time points, ranging from 5 min to 12 h, following injection of particles, 10 μL of blood was drawn *via* the tail nicking method and placed in 5 mL of Solvable (PerkinElmer) at 60 °C overnight for circulation studies. At 30 min and 12 h following injection, mice were sacrificed *via* CO_2 overdose and known organ weights were harvested and placed in 5 mL of Solvable (PerkinElmer) at 60 °C overnight. The next morning, 10 mL of Ultima Gold was added to each sample and 3H content was measured *via* a Packard TriCarb 2100TR scintillation counter. Blood values reported in the 30 min biodistribution studies correspond to a different set of animals than those reported in the circulation studies because the circulation studies required blood samples from multiple time points past 30 min. Blood values reported for 12 h studies

correspond to the same animals as those used for 12 h biodistribution studies.

Two-Compartment Pharmacokinetic Model. A two-compartment pharmacokinetic model was fit to the circulation data with Matlab using nonlinear regression. The model shows excellent agreement with the experimental data for both particle types. From the fitted parameters, pharmacokinetics parameters, including the elimination and distribution half-lives, and volume of distribution were determined, as previously described.[27] The area under the curve concentrations were determined by integrating the model fits over the first 12 h and infinite time and normalized to particle number with the injected dose. The clearance rates and *y*-axis values were also normalized to the injected mass of particles and the compartment volume as described: $C\sim = (V_C/m)(Ae^{\alpha t} + Be^{\beta t})$.

Cellular Uptake Studies. The bEnd.3 endothelial cells and J774 macrophages were incubated at 37 °C in 5% CO_2 in high glucose Dulbecco's modified Eagle's medium, 10% fetal bovine serum (FBS), and 1% penicillin/streptomycin. 4T1 epithelial cells were incubated at 37 °C in 5% CO_2 in RPMI media, 10% FBS, and 1% penicillin/streptomycin. The bEnd.3 cells were stimulated with LPS at a concentration of 5 μg/mL for 18 h. LPS-stimulated bEnd.3 cells were washed of free LPS prior to nanoparticle internalization studies. For quantification of ICAM receptor on the bEnd.3 surface, 500 μg of fluorescent anti-ICAM-1 antibody was incubated with LPS-stimulated cells for 1 h. Cells were lysed *via* multiple freeze−thaw cycles and pelleted, and the supernatant was measured for fluorescence using a Tecan plate reader. Particles (1×10^{11}) in 500 μL of media were pipetted onto confluent cells in 24-well plates. At various time points, ranging from 5 min to 12 h, following addition of particles, medium containing particles was removed from cells and the wells were subsequently washed three times with fresh medium. Then, 500 μL of Solvable was then added to each well and added to 10 mL of Ultima Gold, where 3H content was measured *via* a Packard TriCarb 2100TR scintillation counter.

Conflict of Interest: The authors declare no competing financial interest.

Acknowledgment. A.C.A. was supported by the National Science Foundation Graduate Research Fellowship under Grant No. DGE-1144085 and also by UCSB's Center for Bioengineering under the Mellichamp Fellowship for Graduate Students. M.Z. was supported by the UCSB Crossroads Fellowship. This work was funded in part by the Defense Threat Reduction Agency under the Natick Soldier Research, Development and Engineering Center Agreement No. W911QY-13-2-0001. Characterization was carried out in part in the CNSI facilities at UCSB.

Supporting Information Available: Additional figures. This material is available free of charge *via* the Internet at http://pubs.acs.org.

REFERENCES AND NOTES

1. Mitragotri, S.; Lahann, J. Physical Approaches to Biomaterial Design. *Nat. Mater.* **2009**, *8*, 15–23.
2. Mitragotri, S.; Lahann, J. Materials for Drug Delivery: Innovative Solutions To Address Complex Biological Hurdles. *Adv. Mater.* **2012**, *24*, 3717–3723.
3. Slack, J. D.; Kanke, M.; Simmons, G. H.; Deluca, P. P. Acute Hemodynamic Effects and Blood Pool Kinetics of Polystyrene Microspheres Following Intravenous Administration. *J. Pharm. Sci.* **1981**, *70*, 660–664.
4. Decuzzi, P.; Godin, B.; Tanaka, T.; Lee, S.-Y.; Chiappini, C.; Liu, X.; Ferrari, M. Size and Shape Effects in the Biodistribution of Intravascularly Injected Particles. *J. Controlled Release* **2010**, *141*, 320–327.
5. Moghimi, S. M.; Hunter, A. C.; Murray, J. C. Nanomedicine: Current Status and Future Prospects. *FASEB J.* **2005**, *19*, 311–330.
6. Jain, R. K. Transport of Molecules, Particles, and Cells in Solid Tumors. *Annu. Rev. Biomed. Eng.* **1999**, *1*, 241–263.
7. Choi, H. S.; Liu, W.; Misra, P.; Tanaka, E.; Zimmer, J. P.; Ipe, B. I.; Bawendi, M. G.; Frangioni, J. V. Renal Clearance of Quantum Dots. *Nat. Biotechnol.* **2007**, *25*, 1165–1170.
8. Couvreur, P. Nanoparticles in Drug Delivery: Past, Present and Future. *Adv. Drug Delivery Rev.* **2013**, *65*, 21–23.
9. Champion, J. A.; Katare, Y. K.; Mitragotri, S. Particle Shape: A New Design Parameter for Micro- and Nanoscale Drug Delivery Carriers. *J. Controlled Release* **2007**, *121*, 3–9.
10. Tao, L.; Hu, W.; Liu, Y.; Huang, G.; Sumer, B. D.; Gao, J. Shape-Specific Polymeric Nanomedicine: Emerging Opportunities and Challenges. *Exp. Biol. Med.* **2011**, *236*, 20–29.
11. Muro, S.; Garnacho, C.; Champion, J. A.; Leferovich, J.; Gajewski, C.; Schuchman, E. H.; Mitragotri, S.; Muzykantov, V. R. Control of Endothelial Targeting and Intracellular Delivery of Therapeutic Enzymes by Modulating the Size and Shape of ICAM-1-Targeted Carriers. *Mol. Ther.* **2008**, *16*, 1450–1458.
12. Anselmo, A. C.; Modery-Pawlowski, C. L.; Menegatti, S.; Kumar, S.; Vogus, D. R.; Tian, L. L.; Chen, M.; Squires, T. M.; Sen Gupta, A.; Mitragotri, S. Platelet-like Nanoparticles: Mimicking Shape, Flexibility, and Surface Biology of Platelets To Target Vascular Injuries. *ACS Nano* **2014**, *8*, 11243–11253.
13. Geng, Y.; Dalhaimer, P.; Cai, S.; Tsai, R.; Tewari, M.; Minko, T.; Discher, D. E. Shape Effects of Filaments *versus* Spherical Particles in Flow and Drug Delivery. *Nat. Nanotechnol.* **2007**, *2*, 249–255.
14. Kolhar, P.; Anselmo, A. C.; Gupta, V.; Pant, K.; Prabhakarpandian, B.; Ruoslahti, E.; Mitragotri, S. Using Shape Effects To Target Antibody-Coated Nanoparticles to Lung and Brain Endothelium. *Proc. Natl. Acad. Sci. U.S.A.* **2013**, *110*, 10753–10758.
15. Decuzzi, P.; Ferrari, M. The Adhesive Strength of Non-spherical Particles Mediated by Specific Interactions. *Biomaterials* **2006**, *27*, 5307–5314.
16. Gratton, S. E.; Ropp, P. A.; Pohlhaus, P. D.; Luft, J. C.; Madden, V. J.; Napier, M. E.; DeSimone, J. M. The Effect of Particle Design on Cellular Internalization Pathways. *Proc. Natl. Acad. Sci. U.S.A.* **2008**, *105*, 11613–11618.
17. Champion, J. A.; Mitragotri, S. Shape Induced Inhibition of Phagocytosis of Polymer Particles. *Pharm. Res.* **2009**, *26*, 244–249.
18. Champion, J. A.; Mitragotri, S. Role of Target Geometry in Phagocytosis. *Proc. Natl. Acad. Sci. U.S.A.* **2006**, *103*, 4930–4934.
19. Gilbert, J. B.; O'Brien, J. S.; Suresh, H. S.; Cohen, R. E.; Rubner, M. F. Orientation-Specific Attachment of Polymeric Microtubes on Cell Surfaces. *Adv. Mater.* **2013**, *25*, 5948–5952.
20. Discher, D. E.; Mooney, D. J.; Zandstra, P. W. Growth Factors, Matrices, and Forces Combine and Control Stem Cells. *Science* **2009**, *324*, 1673–1677.
21. Geiger, B.; Spatz, J. P.; Bershadsky, A. D. Environmental Sensing through Focal Adhesions. *Nat. Rev. Mol. Cell Biol.* **2009**, *10*, 21–33.
22. Vogel, V.; Sheetz, M. P. Cell Fate Regulation by Coupling Mechanical Cycles to Biochemical Signaling Pathways. *Curr. Opin. Cell Biol.* **2009**, *21*, 38–46.
23. Engler, A. J.; Sen, S.; Sweeney, H. L.; Discher, D. E. Matrix Elasticity Directs Stem Cell Lineage Specification. *Cell* **2006**, *126*, 677–689.
24. Discher, D. E.; Janmey, P.; Wang, Y.-l. Tissue Cells Feel and Respond to the Stiffness of Their Substrate. *Science* **2005**, *310*, 1139–1143.
25. Griffin, M. A.; Sen, S.; Sweeney, H. L.; Discher, D. E. Adhesion−Contractile Balance in Myocyte Differentiation. *J. Cell Sci.* **2004**, *117*, 5855–5863.
26. Kong, H. J.; Liu, J.; Riddle, K.; Matsumoto, T.; Leach, K.; Mooney, D. J. Non-viral Gene Delivery Regulated by Stiffness of Cell Adhesion Substrates. *Nat. Mater.* **2005**, *4*, 460–464.
27. Merkel, T. J.; Jones, S. W.; Herlihy, K. P.; Kersey, F. R.; Shields, A. R.; Napier, M.; Luft, J. C.; Wu, H.; Zamboni, W. C.; Wang, A. Z.; Bear, J. E.; DeSimone, J. M. Using Mechanobiological Mimicry of Red Blood Cells To Extend Circulation Times of Hydrogel Microparticles. *Proc. Natl. Acad. Sci. U.S.A.* **2011**, *108*, 586–591.
28. Merkel, T. J.; Chen, K.; Jones, S. W.; Pandya, A. A.; Tian, S.; Napier, M. E.; Zamboni, W. E.; DeSimone, J. M. The Effect of

Particle Size on the Biodistribution of Low-Modulus Hydrogel Print Particles. *J. Controlled Release* **2012**, *162*, 37–44.
29. Haghgooie, R.; Toner, M.; Doyle, P. S. Squishy Non-spherical Hydrogel Microparticles. *Macromol. Rapid Commun.* **2010**, *31*, 128–134.
30. Anton, N.; Benoit, J.-P.; Saulnier, P. Design and Production of Nanoparticles Formulated from Nano-emulsion Templates—A Review. *J. Controlled Release* **2008**, *128*, 185–199.
31. Landfester, K.; Musyanovych, A. Hydrogels in Miniemulsions. In *Chemical Design of Responsive Microgels*; Springer: Berlin, 2011; pp 39−63.
32. Steinhilber, D.; Seiffert, S.; Heyman, J. A.; Paulus, F.; Weitz, D. A.; Haag, R. Hyperbranched Polyglycerols on the Nanometer and Micrometer Scale. *Biomaterials* **2011**, *32*, 1311–1316.
33. Hamidi, M.; Azadi, A.; Rafiei, P. Hydrogel Nanoparticles in Drug Delivery. *Adv. Drug Delivery Rev.* **2008**, *60*, 1638–1649.
34. Anselmo, A. C.; Gupta, V.; Zern, B. J.; Pan, D.; Zakrewsky, M.; Muzykantov, V.; Mitragotri, S. Delivering Nanoparticles to Lungs While Avoiding Liver and Spleen through Adsorption on Red Blood Cells. *ACS Nano* **2013**, *7*, 11129–11137.
35. Howard, M.; Zern, B. J.; Anselmo, A. C.; Shuvaev, V. V.; Mitragotri, S.; Muzykantov, V. Vascular Targeting of Nanocarriers: Perplexing Aspects of the Seemingly Straightforward Paradigm. *ACS Nano* **2014**, *8*, 4100–4132.
36. Hayes, S. H.; Seigel, G. M. Immunoreactivity of ICAM-1 in Human Tumors, Metastases and Normal Tissues. *Int. J. Clin. Exp. Pathol.* **2009**, *2*, 553–560.
37. duPre, S. A.; Redelman, D.; Hunter, K. W., Jr. Microenvironment of the Murine Mammary Carcinoma 4T1: Endogenous IFN-γ Affects Tumor Phenotype, Growth, and Metastasis. *Exp. Mol. Pathol.* **2008**, *85*, 174–188.
38. Lawson, C.; Wolf, S. ICAM-1 Signaling in Endothelial Cells. *Pharmacol. Rep.* **2009**, *61*, 22–32.
39. Sikorski, E.; Hallmann, R.; Berg, E.; Butcher, E. The Peyer's Patch High Endothelial Receptor for Lymphocytes, the Mucosal Vascular Addressin, Is Induced on a Murine Endothelial Cell Line by Tumor Necrosis Factor-Alpha and Il-1. *J. Immunol.* **1993**, *151*, 5239–5250.
40. Scott, G. S.; Kean, R. B.; Fabis, M. J.; Mikheeva, T.; Brimer, C. M.; Phares, T. W.; Spitsin, S. V.; Hooper, D. C. ICAM-1 Upregulation in the Spinal Cords of Plsjl Mice with Experimental Allergic Encephalomyelitis Is Dependent upon TNF-α Production Triggered by the Loss of Blood−Brain Barrier Integrity. *J. Neuroimmunol.* **2004**, *155*, 32–42.
41. Ravetch, J. V.; Bolland, S. IgG Fc Receptors. *Annu. Rev. Immunol.* **2001**, *19*, 275–290.
42. Moghimi, S. M.; Hunter, A. C.; Murray, J. C. Long-Circulating and Target-Specific Nanoparticles: Theory to Practice. *Pharmacol. Rev.* **2001**, *53*, 283–318.
43. Owens, D. E., III; Peppas, N. A. Opsonization, Biodistribution, and Pharmacokinetics of Polymeric Nanoparticles. *Int. J. Pharm.* **2006**, *307*, 93–102.
44. Dhillon, S.; Gill, K. Basic Pharmacokinetics. In *Clinical Pharmacokinetics*; Pharmaceutical Press: London, 2006; pp 1−44.
45. Herant, M.; Heinrich, V.; Dembo, M. Mechanics of Neutrophil Phagocytosis: Behavior of the Cortical Tension. *J. Cell Sci.* **2005**, *118*, 1789–1797.